Lawrence Berkeley National Laboratory
Recent Work

Title
In Situ Transmission Electron Microscopy of Cadmium Selenide Nanorod Sublimation

Permalink
https://escholarship.org/uc/item/6jd4542b

Journal
The Journal of Physical Chemistry Letters, 6(4)

ISSN
1948-7185

Authors

Hellebusch, Daniel J.
Manthiram, Karthish
Beberwyck, Brandon J.
et al.

Publication Date
2015-02-19

In Situ Transmission Electron Microscopy of Cadmium Selenide Nanorod Sublimation

Daniel J. Hellebusch†[″][#]**, Karthish Manthiram†**[#]**, Brandon J. Beberwyck‡**[″][#]**, and A. Paul Alivisatos**[*]**‡§**[″][#]

[†]Department of Chemical and Biomolecular Engineering, [‡]Department of Materials Science and Engineering, and [§]Department of Chemistry, University of California, Berkeley, Berkeley, California 94720, United States

[″] Materials Sciences Division, Lawrence Berkeley National Laboratory, Berkeley, California 94720, United States

[#] Kavli Energy Nanosciences Institute, University of California, Berkeley and Lawrence Berkeley National Lab, Berkeley, California 94720, United States

*E-mail: alivis@berkeley.edu.

•

Abstract
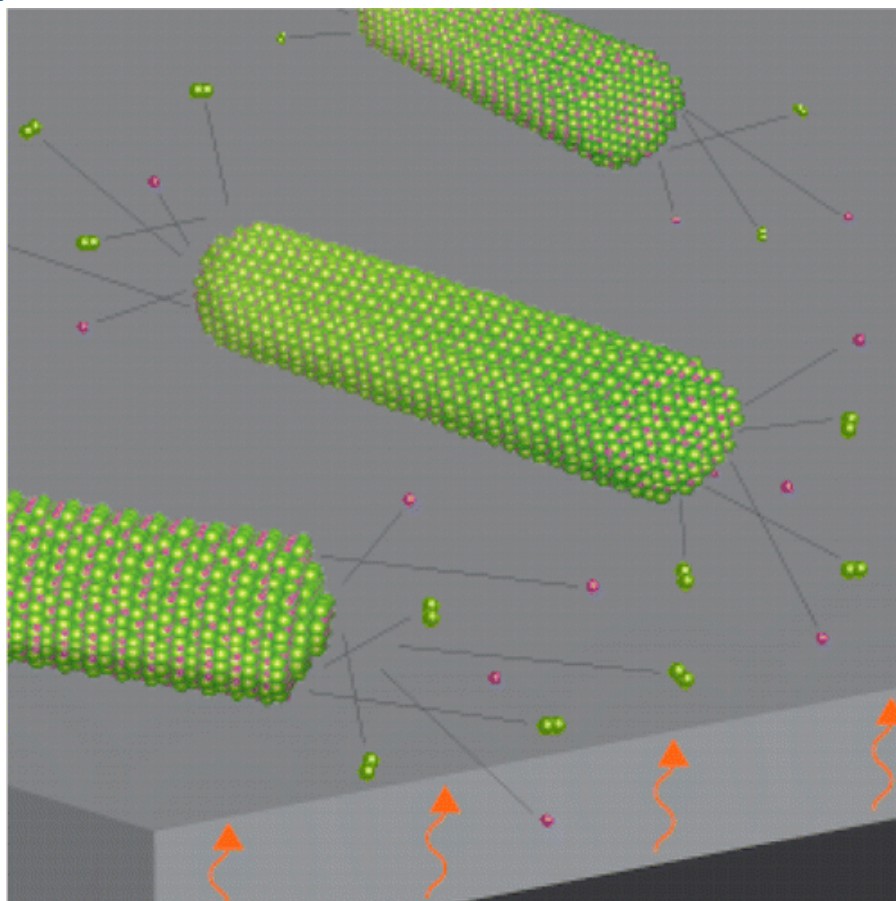
In situ electron microscopy is used to observe the morphological evolution of cadmium selenide nanorods as they sublime under vacuum at a series of elevated temperatures. Mass loss occurs anisotropically along the nanorod's long axis. At temperatures close to the sublimation threshold, the phase change occurs from both tips of the nanorods and proceeds unevenly with periods of rapid mass loss punctuated by periods of relative stability. At higher temperatures, the nanorods sublime at a faster, more uniform rate, but mass loss occurs from only a single end of the rod. We propose a mechanism that accounts for the observed sublimation behavior based on the terrace–ledge–kink (TLK) model and how the nanorod surface chemical environment influences the kinetic barrier of sublimation.

Despite many advances in the study of nanostructured materials, it remains challenging to develop descriptions of the thermodynamic, and kinetic factors that lead a given nanostructure to be as stable as these materials are typically in nonequilibrium states. In the case of colloidal nanocrystals, valuable insight into their stability has often come from studies of the transformation of their size, shape, and faceting during growth.[1, 2] Such studies have been greatly expanded recently with the advent of high-resolution real-time electron microscopy for in situ characterization. Nanoparticle growth,[3-5] coalescence,[6, 7] and phase changes, including melting,[8, 9] sublimation,[8, 10-13] and crystallographic transformations,[14] have been investigated at the single-particle level, providing valuable information on the stability and formation of these structures. Collectively, these studies begin to describe how these kinetically trapped structures are influenced by the nature of their surface modifications, with ligands playing a key role in manipulating interfacial energies and contributing to stabilization. Here, we investigate the sublimation of nanorods. In addition to providing insight into facet stability, observing the sublimation of nanocrystals may serve as a useful complementary approach to directly observing the growth of nanocrystals. While growth and sublimation may occur under different thermodynamic conditions such as pressure, sublimation can shed light on the growth mechanisms if the microscopic steps for the inverse and forward processes are similar. The extension to anisotropic structures offers the opportunity to better understand the relative stability of the diverse crystal facets. We chose to study cadmium chalcogenide (CdE, E = S, Se, Te) nanocrystals because their physical and chemical properties have been extensively studied. CdE nanostructures have been applied to a variety of optical and optoelectronic applications such as display phosphors,[15] biological markers,[16] and photovoltaics.[17] Early studies of colloidal II–VI structures focused on dots, or nearly spherical shapes, until approaches to make nanorods were developed. Nanorods form under similar conditions to quantum dots except for the presence of a selectively binding surface ligand, which is believed to retard the growth of one set of facets relative to the others.[2] Anisotropic nanostructures provide a

means for building more complex, directional nanostructures sequentially,[18, 19] and their broken symmetry leads to optical and electronic properties distinct from their spherical counterparts, including polarized emission[20] and enhanced absorption and charge transport.[21] Exploring sublimation provides insight into facet stability and the influence of surface ligands on these anisotropic nanostructures. Here, we study the sublimation of one such model system, CdSe nanorods.

In this work, we present direct imaging of sublimation in CdSe nanorods under vacuum at a series of temperatures below and above the bulk transition temperature. At the TEM column pressures of 10^{-7} Torr, the sublimation point is predicted to be 389 ± 5 °C;[22] we studied sublimation at 370, 390, 420, and 450 °C. Colloidal CdSe nanorods with a wurtzite crystallographic structure were synthesized following methods established in the literature. The tetradecylphosphonate surfactant retards growth on the nonpolar $(10\bar{1}0)$ and $(11\bar{2}0)$ facets; therefore, growth occurs along the c-axis that is parallel or antiparallel to the [0001] direction.[23] A dilute solution of nanorods dispersed in toluene was drop-casted onto a commercially available, low thermal drift TEM grid and, sublimation of these nanostructures was recorded. The temperature ramp rate for these grid was 10^{6} °C/s, permitting virtually isothermal heating conditions. Videos of CdSe nanorod sublimation at 370, 390, 420, and 450 °C can be found in Videos S1–S4, and selected frames can be found in Figure S1 in the Supporting Information (SI).

Nanorod sublimation proceeded anisotropically from the ends along the c-axis of the wurtzite crystal structure. We identify the observed phenomena as sublimation because no remnant of a solid, which would manifest as mass–thickness contrast in the TEM image, formed upon the cooling substrate. CdSe nanorod sublimation dynamics at 370 °C is represented in Figure 1, which contains four video frames from Video S1 SI. The bottom row of images of Figure 1 are digitally processed images complementary to the top row to aid in visualizing sublimation progress. The images in Figure 1 show that the nanorods decrease in length due to sublimation, which initiates at the tips and continues along the length of the particle. At this low temperature, mass loss occurred from both ends of the nanorods. At higher temperatures, sublimation occurred exclusively from one end of the nanorod. Figure 2 shows this effect at 450 °C.
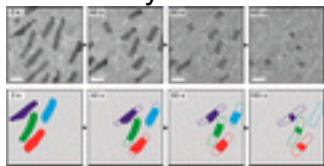

Figure 1. (Top) Bright-field TEM video frames showing the progression of nanorod sublimation at 370 °C. (Bottom) Qualitative image maps with initial nanorod profiles at $t = 0$ s shown as dotted outlines and profiles at the specified time shown as a solid fill. The scale bar is 10 nm.
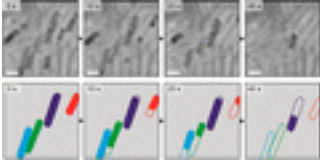
Figure 2. (Top) Bright-field TEM video frames at increasing times showing the progression of sublimation from one end of the nanorod at 450 °C. (Bottom) Qualitative image maps with initial nanorod profiles at t = 0 s shown as dotted outlines and profiles at the specified time shown as a solid fill. The scale bar is 10 nm.

At the lowest temperature, 370 °C, nanorod sublimation occurred at a temperature below the predicted bulk sublimation point at the TEM column pressures. Sublimation at this temperature would only initiate after imaging a given field of view. This e-beam phase change induction was not observed at higher temperatures. For example, partially sublimed nanorods are seen at the start of the videos at the higher temperatures but not at the lowest.

At all observed temperatures, nanorods generally sublimed anisotropically, losing mass along the c-axis until the particle reached 2–3 nm in length measured along the c-axis. Before reaching this transition size, the rod diameter did not change within resolution limits. Upon reaching this transition size, the sublimation direction changed from the c-axis to the ab-axes and quickly proceeded from one side of the nanorod until no crystal remained. Our analysis will be confined to what happens above this transition size because below the transition, it is difficult to quantify the size of the residual nanocrystals. To quantify the sublimation dynamics above the transition size, we measured the dimensions of four nanorods at each temperature throughout the videos that are identified in Figure S2 (SI). Because nanorod widths did not change within resolution limits of the data up until the transition point, we used the rate of linear length decrease along the c-axis of the nanorod to calculate mass loss; see Figure S3 (SI) for a schematic of our measurement method.

The average sublimation rate increased with temperature, as shown in Figure 3. Uncertainty in the rate of sublimation from individual nanorods precludes us from demonstrating if the sublimation follows Arrhenius kinetics and from obtaining an accurate activation energy. Variations in the pattern of sublimation at low and high temperatures could be seen very clearly, however.
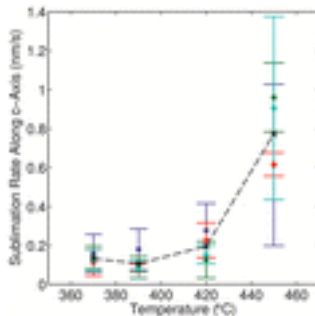
Figure 3. Average sublimation rate along the *c*-axis direction for four nanorods at different temperatures. Rates were averaged from both ends during the entire phase change for each nanorod; error bars represent the standard deviation. Black "X" markers and the dashed line indicate the average rate for all nanorods at all times for each temperature.

The sublimation rate from the nanorod ends is not always continuous and is strongly dependent on temperature. There are two distinct behaviors, (1) noncontinuous, punctuated sublimation from *both* ends at low temperatures, and (2) continuous sublimation from *one* end at high temperatures. The intermediate temperatures exhibited a mixture of these modes. Noncontinuous behavior is defined by sporadic pauses occurring locally at a single nanorod end during the course of sublimation. Figure 1 shows that all nanorods sublime from both ends at 370 °C. By 450 °C, the sublimation only proceeds from one end of the nanorod, as seen in Figure 2. This is accompanied by an increased rate of mass loss established in Figure 3. Figure 4 reports the cumulative length sublimed from each end of the four measured nanorods at their respective temperatures using the same methodology as that established above.
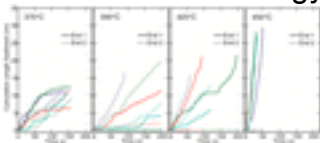

Figure 4. Total length sublimed from the ends of each nanorod. Each color represents a different nanorod, as indicated in Figure S2 (SI), which also correspond to colors in Figure 2. The two ends are differentiated by the solid (end closer to the top of the frame) and dashed lines (end closer to the bottom of the frame) in the orientation in Figure S2 (SI).

During sublimation, the solid interface at the nanorod end, or the sublimation front, rocked back and forth as mass vaporized. This interface is defined as a difference in contrast between the nanocrystal and the substrate spanning the width of the nanorod at each tip. As a given sublimation front progressed along the length of the particle, the interface made an angle greater or less than the normal with the *c*-axis. One side of the front might progress while the opposite remains stationary and appears "pinned", creating an angle with the *c*-axis normal. The active front exhibiting this behavior would switch from side to side, creating a rocking or seesaw appearance. This was observed at all temperatures. At the lower temperatures, both sides of the sublimation front would sometimes periodically halt, sometimes ending in what appeared to be a pristine facet from the TEM image.

The single particle in situ electron microscopy sublimation studies shown here enable us to see phenomena that would be entirely obscured in ensemble studies. Here, there are two rather surprising observations; on the one hand, sublimation is punctuated but proceeds from both ends of the rods at low temperature, while on the other, sublimation is continuous but occurs from only one end of a rod at higher temperature. While these observations beg for a clear

mechanistic explanation, the fact is that the in situ TEM employed here has limitations that allow us, for the time being only, to provide competing viewpoints that will require further exploration to distinguish between. In what follows, we first present a mechanism that relies solely upon what we know about the idealized intrinsic material comprising the nanocrystals as synthesized. This is followed by a more complex explanation that relies upon nonideal changes in the surface species bound to the nanoparticles induced by the electron beam. Both perspectives focus on elucidating how the kinetic barrier of a desorbing surface species—the rate limiting step—is modified by its coordinating environment. A more complete picture of the sublimation process that distinguishes between these two classes of explanations, ideal and nonideal, or that even involves a combination of the two must await a new technique that enables simultaneous observation of the surface species on the nanocrystal while it is under observation in the microscope.

To understand the idealized mechanism of CdSe nanorods, we first explore sublimation in an ideal crystal lattice model. Past mechanistic insights on sublimation in bulk II–VI compounds invoke the terrace–ledge–kink model (TLK) of solid surfaces. The sublimation reaction begins when a CdSe unit moves from a terrace to a ledge site and then to a kink site where it dissociates into neutral adsorbates via charge transfer followed by desorption.[24-27] This series of reactions is reversible and in the opposite direction provides a description of crystal growth. There is disagreement in the literature on whether charge transfer or desorption is the rate-limiting step for cadmium chalcogenides.[24-30] In the context of CdSe nanorod sublimation, we consider a simplified reaction mechanism in which understanding what influences the activation barrier of the rate-limiting step—either charge transfer or desorption—is key to understanding the observed sublimation behavior. Below, we will discuss how the coordination environment of the surface CdSe unit may affect this activation barrier.

In a pure CdSe crystal, the rate-limiting step is slow when the surface unit has a high coordination number, such as a site on a pristine facet or a terrace in the TLK model, compared to a low coordination site, such as a kink. Past investigations in bulk crystals found that the limiting step occurred fastest at a kink site.[24-30] Mass loss is expected to be faster from a surface with a large population of kink sites and slower from a surface populated with ledges and terraces. When the crystal is less than ideal, defects may also play an important role in sublimation by reducing the activation energy of sublimation. For example, a higher concentration of vacancies increases the probability of lower-coordinated CdSe units, while twinning and stacking faults produce strain in a lattice, reducing the bonding energy with adjacent atoms.

We add a level of complexity to this model crystal by considering an ideal ligand shell. Nanorods are distinct from bulk crystals by possessing a high ratio of surface to interior atoms, which are subject to coordination to other molecules such as ligands. Because it has been established that the coordination environment of surface species determines the sublimation rate, we must explore

how binding to these other species influences the kinetic barrier. First-principles calculations of the relative surface energies of ligand-passivated facets show that the polar {0001} facets of a bare CdSe nanorod with a relaxed and reconstructed surface have a higher surface energy compared to the nonpolar sides.(31-33) Coordinating the wurtzite CdSe surfaces with methyl phosphonic acid—a ligand similar to the species in our system—further increased the stability of the nonpolar sides relative to the tips; the former were shown to be most stable upon ligand passivation.(32-36)

In view of the factors above that can influence the kinetic barrier to sublimation, we first propose an idealized mechanism for the observed phase transition behavior. Sublimation initiates when a CdSe unit positioned at a high-energy surface site on the nanorod end undergoes charge transfer and desorbs. We suspect that this occurs at a site that is not coordinated by a surface ligand as calculations show methylphosphonic acid does not completely passivate the polar end facets.(32) The departure of this initial unit produces lower coordinated sites such as kinks, which will sublime, yielding additional kinks and ultimately leading to a surface rich in kinks; this is a nucleation event in the phase transition.

At 370 °C, sublimation was observed at a temperature below the predicted bulk transition point. The electron beam played a role in initiating sublimation because the phase transformation initiated only after illumination. Incident electrons can transfer kinetic energy, resulting in sample heating, or simply increase charge concentration in CdSe, therefore promoting charge transfer between the heteroatoms.(11, 14, 26, 37) Depending on the nature of the rate-limiting step, both effects assist in overcoming a potential barrier for the phase change and lead to sublimation below the predicted bulk transition point. We cannot rule out phase transition size effects, such as the melting point suppression in spherical CdS nanocrystals.(38) However, the depression of the melting temperature is less pronounced in asymmetrical structures such as nanowires.(39, 40)

Once sublimation is induced at the nanorod tip, the mass loss continues along the c-axis of the nanorods at an interface rich in kink sites. This behavior is consistent with the calculations discussed above; the nonpolar facets that comprised the nanorod sides are greatly stabilized by coordination with the ligands compared to the ends, favoring mass loss along the c-axis. This anisotropic behavior corroborates past experimental observations of sublimation from single crystals. In CdSe/CdS octapods, the CdS arms sublimed along the c-axis.(41) In bulk wurtzite CdS, sublimation from the bulk (0001) face was found to be faster than the nonpolar $(10\bar{1}0)$ face but only by a factor of less than two.(42) In rocksalt PbS nanocrystals, sublimation occurred faster from the polar {111} facets than the nonpolar {001} surfaces, and ligand passivation was suggested to play a role.(8) The strong ligand stabilization of the side atoms is also likely responsible for the "pinning" of the side atoms that results in the rocking behavior of the sublimation fronts as well as post-transition size sublimation behavior. In both cases, cadmium phosphonate strongly bonds to the CdSe units on the

nonpolar facets, increasing the barrier to sublimation. A similar behavior was observed directly in the TEM in silver cubes (sides ~100 nm); surface interaction by the polymer ligand shell influences the facet order of sublimation.(10)

A mechanism based upon an idealized nanorod–ligand model can be invoked to describe the two sublimation behaviors. Whether a phase change occurs from both or one end is dependent on temperature, but other factors such as ligand surface pinning at the nanorod tips and the asymmetry of the crystal may also play a role. At the higher temperature, the sublimation still initiates from the nanorod end. If the potential barrier imposed by the ligand is not as strongly influenced by temperature as sublimation, then it is possible that at the highest temperatures, once the phase change is initiated at one end, the sublimation rate is so rapid that the rod vaporizes before the opposite rod end can nucleate. The asymmetry in the nanorod may exacerbate this effect. For instance, the calculations mentioned above revealed that the $(000\bar{1})$ face prefers no ligand passivation and is less stable than the opposite (0001), which maintains partial passivation.(32, 33) Furthermore, the wurtzite CdSe crystal lacks an inversion center along the c-axis, creating two different bonding environments for atoms at the (0001) and $(000\bar{1})$; on an unreconstructed surface, cadmiums bond to three selenium atoms on the (0001) surface but have only one bond on the $(000\bar{1})$ face. In fact, past investigations suggest that the $[000\bar{1}]$ is the direction of growth.(28-30, 43) If this applies to sublimation, than we expect mass loss to occur faster in this direction. However, we cannot distinguish between the two facets within the resolution of our images.

The punctuated versus continuous sublimation behavior observed can be explained by the perturbation of the kinetic barrier of the surface CdSe units. Similar nonuniform sublimation behavior was observed in silver and PbS nanocrystals.(8, 11) Van Huis et al. attributed pauses in PbS to the stochastic nature of microscopic processes and ligand passivation of particular facets.(8) Asoro et al. suggested a mechanism whereby the nanocrystal fractures along a low-energy facet create a small fragment that then rapidly vaporizes due to its large surface area.(8, 11) Because of the limits of our frame rate and image resolution, we cannot assess if the latter process applies. One might suspect that the pauses observed at the lower temperatures may be induced by local cooling below the transition point due to the latent heat of sublimation and thus temporarily decrease the sublimation rate. However, the speed of sound in CdSe is $1.5–3.8 \times 10^7$ m/s, which prevents thermal gradients at these length scales.(44)

Invoking our idealized nanocrystal model, we propose a mechanism whereby the punctuated and uniform sublimation rates observed at lower and higher temperature are controlled by the coordination of the surface CdSe units. In an ideal CdSe nanorod end free of surface ligand, the sublimation rate is fast from a surface populated with low coordination sites such as kinks and slow from one dominated by low coordination sites such as ledges or terraces. A clean {0001} facet will cause the rate to "freeze" momentarily until a kink site is nucleated.

Sublimation appears punctuated at low temperatures as the nanorod ends fluctuate between large populations of low coordination sites and high coordination sites and can even pause at the kink-free facet. Temporary basal plane facets can been seen at the nanorod ends at 370 °C in Video S1 (SI); rod A exhibits a sustained {0001} plane at $t = 8$ s (video time ≈ 105 s real time). In the high-temperature regime, only kink sites exist or are easily generated by surface diffusion, and mass loss is continuous. This is consistent with the images that show rounded nanorod tips and the lack of any basal planes at high temperatures. Defects may contribute to the punctuated behavior of the low-temperature regime. As an advancing front encounters defects, sublimation proceeds quickly as these sites have a reduced kinetic barrier. However, we are unable to confirm the presence of defects in our samples due to resolution limits. An equally plausible mechanism based upon nonideal changes in the surface species offers an alternative description of the two sublimation behaviors. When running an in situ experiment inside of the TEM, we must be cognizant of the e-beam effects. High-energy dosages lead to decomposition of the ligand shell and the presence of other unknown contaminants in the column that can modify the nanorod surface and influence the kinetic barrier to sublimation. The presence of a lighter-contrast footprint of the nanorod remained after sublimation, which is indicative of organic deposition. A similar shell was observed in the sublimation of CdS/CdSe octopods and silver cubes.(10, 41) Besides ligands, other species can adsorb to the nanocrystal surface and inhibit the sublimation rate. These species are most likely carbon, but unknown TEM column contaminants from previous experiments cannot be definitively ruled out. The ligand alkyl chains or carbon support can decompose, vaporize, and redeposit as amorphous carbon on the nanorods. Furthermore, alkyl chains have been reported to cross-link under electron beam radiation, which would convert the ligands into stronger-binding, multidentate species.(45-47) We suspect that a carbon shell exists around nanorods in our experiments, and further, this shell need not arise from cross-linking of ligands. Past investigations report that the deposition of polymerized pump oils used in diffusion pumps leads to sublimation retardation in bulk CdS crystals.(42)

A sublimation mechanism based upon nonideal conditions within the TEM can offer a competing viewpoint to the ideal model. Contaminants deposited on the nanorod surface would increase the kinetic barrier of the rate-limiting step, which could potentially reduce the rate of mass loss from the tips. At lower temperatures, it is possible that the sublimation rate may be similar to the contaminant deposition rate. If this is correct, then the sublimation front would pause when contaminants deposit and then continue after the surface "unpins" from the contaminant via nucleation or desorption of the foreign species. At higher temperatures, sublimation might occur much faster than deposition, resulting in continuous mass loss. Clearly, further experiments are needed to test this hypothesis.

We observed that CdSe nanorods sublime anisotropically along the direction of

the least stable facet. The sublimation rate, measured along the *c*-axis, increased with temperature. Two distinct behaviors of sublimation were discovered, noncontinuous from both ends at lower temperatures and continuous from one end at higher temperatures. A mechanism that considers the coordination environment of the surface species is explained using two nanocrystal models, ideal and nondeal, that can potentially account for these results, and further experiments are needed to explain these surprising sublimation observations.

Supporting Information

Sublimation temperature calculation, Figures S1–S4 in PDF form; Videos S1–S4 are separate AVI files. This material is available free of charge via the Internet at http://pubs.acs.org.

⊥ Author Contributions

K.M. and B.J.B. contributed equally to this work.

The authors declare no competing financial interest.

•

• Reference QuickView

•

References

This article references 47 other publications.

1. Glotzer, S. C.; Solomon, M. J.Anisotropy of Building Blocks and Their Assembly into Complex Structures *Nat. Mater.* **2007**, 6, 557–562[CrossRef], [PubMed], [CAS]
2. Yin, Y.; Alivisatos, A. P.Colloidal Nanocrystal Synthesis and the Organic–Inorganic Interface *Nature* **2005**, 437, 664– 670[CrossRef], [PubMed], [CAS]
3. Zheng, H.; Smith, R. K.; Jun, Y.-W.; Kisielowski, C.; Dahmen, U.; Alivisatos, A. P.Observation of Single Colloidal Platinum Nanocrystal Growth Trajectories *Science* **2009**, 324, 1309– 1312[CrossRef], [PubMed], [CAS]
4. Yuk, J. M.; Park, J.; Ercius, P.; Kim, K.; Hellebusch, D. J.; Crommie, M. F.; Lee, J. Y.; Zettl, A.; Alivisatos, A. P.High-Resolution EM of Colloidal

Nanocrystal Growth Using Graphene Liquid Cells *Science* **2012**, 336, 61– 64[CrossRef], [PubMed], [CAS]

5. Liao, H.-G.; Zherebetskyy, D.; Xin, H.; Czarnik, C.; Ercius, P.; Elmlund, H.; Pan, M.; Wang, L.-W.; Zheng, H.Facet Development during Platinum Nanocube Growth *Science* **2014**, 345, 916– 919[CrossRef], [PubMed], [CAS]

6. Lim, T. H.; Mccarthy, D.; Hendy, S. C.; Stevens, K. J.; Brown, S. A.; Tilley, R. D.Real-Time TEM and Kinetic Monte Carlo Studies of the Coalescence of Decahedral Gold Nanoparticles *ACS Nano* **2009**, 3, 3809– 3813[ACS Full Text ⬇], [PubMed], [CAS]

7. Asoro, M. A.; Kovar, D.; Shao-Horn, Y.; Allard, L. F.; Ferreira, P. J.Coalescence and Sintering of Pt Nanoparticles: In Situ Observation by Aberration-Corrected HAADF STEM *Nanotechnology* **2010**, 21, 025701[CrossRef], [CAS]

8. Van Huis, M. A.; Young, N. P.; Pandraud, G.; Creemer, J. F.; Vanmaekelbergh, D.; Kirkland, A. I.; Zandbergen, H. W.Atomic Imaging of Phase Transitions and Morphology Transformations in Nanocrystals *Adv. Mater.* **2009**, 21, 4992– 4995[CrossRef], [PubMed], [CAS]

9. Link, S.; Wang, Z. L.; El-Sayed, M. A.How Does a Gold Nanorod Melt? *J. Phys. Chem. B* **2000**, 104, 7867– 7870[ACS Full Text ⬇], [CAS]

10. Ding, Y.; Fan, F.; Tian, Z.; Wang, Z. L.Sublimation-Induced Shape Evolution of Silver Cubes *Small* **2009**, 5, 2812– 2815[CrossRef], [PubMed], [CAS]

11. Asoro, M. A.; Kovar, D.; Ferreira, P. J.In Situ Transmission Electron Microscopy Observations of Sublimation in Silver Nanoparticles *ACS Nano* **2013**, 7, 7844– 7852[ACS Full Text ⬇], [PubMed], [CAS]

12. Lee, J.-G.; Lee, J.; Tanaka, T.; Mori, H.In Situ HREM Observation of Crystalline-to-Gas Transition in Nanometer-Sized Ag Particles *Phys. Rev. Lett.* **2006**, 96, 075504[CrossRef], [CAS]

13. Yim, J. W. L.; Xiang, B.; Wu, J.Sublimation of GeTe Nanowires and Evidence of Its Size Effect Studied by In Situ TEM *J. Am. Chem. Soc.* **2009**, 131, 14526– 14530[ACS Full Text ⬇], [PubMed], [CAS]

14. Zheng, H.; Rivest, J. B.; Miller, T. A.; Sadtler, B.; Lindenberg, A.; Toney, M. F.; Wang, L.-W.; Kisielowski, C.; Alivisatos, A. P.Observation of Transient Structural-Transformation Dynamics in a Cu_2S Nanorod *Science* **2011**, 333, 206– 209[CrossRef], [PubMed], [CAS]

15. Lee, J.; Sundar, V. C.; Heine, J. R.; Bawendi, M. G.; Jensen, K. F.Full Color Emission Form II–VI Semiconductor Quantum Dot–Polymer Composits *Adv. Mater.* **2000**, 12, 1102– 1105[CrossRef], [CAS]

16. Bruchez, M., Jr.; Morone, M.; Gin, P.; Weiss, S.; Alivisatos, A. P.Semiconductor Nanocrystals as Fluorescent Biological Labels *Science* **1998**, 281, 2013– 2016[CrossRef], [PubMed], [CAS]

17. Kamat, P. V.Quantum Dot Solar Cells. Semiconductor Nanocrystals as Light Harvesters *J. Phys. Chem. C* **2008**, 112, 18737– 18753[ACS Full

Text ⬦], [CAS]

18. Mokari, T.; Rothenberg, E.; Popov, I.; Costi, R.; Banin, U.Selective Growth of Metal Tips onto Semiconductor Quantum Rods and Tetrapods *Science* **2004**, 304, 1787– 1790[CrossRef], [PubMed], [CAS]

19. Talapin, D. V.; Nelson, J. H.; Shevchenko, E. V.; Aloni, S.; Sadtler, B.; Alivisatos, A. P.Seeded Growth of Highly Luminescent CdSe/CdS Nanoheterostructures with Rod and Tetrapod Morphologies *Nano Lett.* **2007**, 7, 2951– 2959[ACS Full Text ⬦], [PubMed], [CAS]

20. Hu, J.; Li, L.-S.; Yang, W.; Manna, L.; Wang, L.-W.; Alivisatos, A. P.Linearly Polarized Emission from Colloidal Semiconductor Quantum Rods *Science* **2001**, 292, 2060– 2063[CrossRef], [PubMed], [CAS]

21. Huynh, W. U.; Dittmer, J. J.; Alivisatos, A. P.Hybrid Nanorod–Polymer Solar Cells *Science* **2002**, 295, 2425– 2427[CrossRef], [PubMed], [CAS]

22. Sharma, R. C.; Chang, Y. A.The Cd–Se (Cadmium–Selenium) System *J. Phase Equilib.* **1996**, 17, 140– 145[CrossRef], [CAS]

23. Peng, Z. A.; Peng, X.Nearly Monodisperse and Shape-Controlled CdSe Nanocrystals via Alternative Routes: Nucleation and Growth *J. Am. Chem. Soc.* **2002**, 124, 3343– 3353[ACS Full Text ⬦], [PubMed], [CAS]

24. Meschi, D. J.; Searcy, A. W.The Kinetics of Dissociative Vaporization Reactions *High Temp. Sci.* **1974**, 6, 221– 236[CAS]

25. Short, D. W.; Rapp, R. A.; Hirth, J. P.Influence of Surface Charge and Surface Structure on the Sublimation of Ionic Crystals *J. Chem. Phys.* **1972**, 57, 1381[CrossRef], [CAS]

26. Somorjai, G. A.Mechanism of Sublimation *Science* **1968**, 162, 755– 760[CrossRef], [PubMed], [CAS]

27. Munir, Z. A.; Hirth, J. P.Transient Phenomena in the Sublimation of Cadmium Sulfide *J. Electron. Mater.* **1977**, 6, 409– 424[CrossRef], [CAS]

28. Munir, Z. A.; Seacrist, L. S.; Hirth, J. P.Morphology of Thermally Etched Basal Surfaces of Cadmium Selenide *Surf. Sci.* **1971**, 28, 357– 372[CrossRef], [CAS]

29. Seacrist, L. S.; Munir, Z. A.Studies on the Sublimation of IIB–VIA Compounds IV. The Anisotropic Behavior of the Sublimation of Basal-Plane Oriented Crystals of Cadmium Selenide *High Temp. Sci.* **1971**, 3, 340– 348[CAS]

30. Leonard, R. B.; Searcy, A. W.The Variation of Vaporization Rates with Orientation for Basal Planes of Zinc Oxide and Cadmium Sulfide *J. Appl. Phys.* **1971**, 42, 4047[CrossRef], [CAS]

31. Puzder, A.; Williamson, A. J.; Zaitseva, N.; Galli, G.; Manna, L.; Alivisatos, A. P.The Effect of Organic Ligand Binding on the Growth of CdSe Nanoparticles Probed by Ab Initio Calculations *Nano Lett.* **2004**, 4, 2361– 2365[ACS Full Text ⬦], [CAS]

32. Manna, L.; Wang, L. W.; Cingolani, R.; Alivisatos, A. P.First-Principles Modeling of Unpassivated and Surfactant-Passivated Bulk Facets of Wurtzite CdSe: A Model System for Studying the Anisotropic Growth of

CdSe Nanocrystals *J. Phys. Chem. B* **2005**, 109, 6183– 6192[ACS Full Text ◆], [PubMed], [CAS]

33. Rempel, J. Y.; Trout, B. L.; Bawendi, M. G.; Jensen, K. F.Properties of the CdSe(0001), (0001), and (1120) Single Crystal Surfaces: Relaxation, Reconstruction, and Adatom and Admolecule Adsorption *J. Phys. Chem. B* **2005**, 109, 19320– 19328[ACS Full Text ◆], [PubMed], [CAS]

34. Hughes, S. M.; Alivisatos, A. P.Anisotropic Formation and Distribution of Stacking Faults in II–VI Semiconductor Nanorods *Nano Lett.* **2013**, 13, 106– 110[ACS Full Text ◆], [PubMed], [CAS]

35. Talapin, D. V.; Shevchenko, E. V.; Murray, C. B.; Kornowski, A.; Förster, S.; Weller, H.CdSe and CdSe/CdS Nanorod Solids *J. Am. Chem. Soc.* **2004**, 126, 12984– 12988[ACS Full Text ◆], [PubMed], [CAS]

36. Manna, L.; Scher, E. C.; Li, L.-S.; Alivisatos, A. P.Epitaxial Growth and Photochemical Annealing of Graded CdS/ZnS Shells on Colloidal CdSe Nanorods *J. Am. Chem. Soc.* **2002**, 124, 7136– 7145[ACS Full Text ◆], [PubMed], [CAS]

37. Hobbs, L. W. Radiation Effects with Inorganic Specimens. In *Introduction to Analytical Electron Microscopy*; Hren, J. J.; Goldstein, J. I.; Joy, D. C., Eds.; Plemnum Press: New York, **1979**; pp 437– 480.[CrossRef]

38. Goldstein, A. N.; Echer, C. M.; Alivisatos, A. P.Melting in Semiconductor Nanocrystals *Science* **1992**, 256, 1425– 1427[CrossRef], [PubMed], [CAS]

39. Goswami, G. K.; Nanda, K. K.Comment on "Size-Dependent Melting Behavior of Zn Nanowire Arrays" [Appl. Phys. Lett. 88, 173114 (2006)] *Appl. Phys. Lett.* **2007**, 91, 196101[CrossRef], [CAS]

40. Gulseren, O.; Ercolessi, F.; Tosatti, E.Premelting of Thin Wires *Phys. Rev. B* **1995**, 51, 7377– 7380[CrossRef], [PubMed], [CAS]

41. Goris, B.; Van Huis, M. a.; Bals, S.; Zandbergen, H. W.; Manna, L.; Van Tendeloo, G.Thermally Induced Structural and Morphological Changes of CdSe/CdS Octapods *Small* **2012**, 8, 937– 942[CrossRef], [PubMed], [CAS]

42. Somorjai, G. A.; Stemple, N. R.Orientation Dependence of the Evaporation Rate of CdS Single Crystals *J. Appl. Phys.* **1964**, 35, 3398[CrossRef], [CAS]

43. Lam, S.-T. *A Unified Approach to the Vaporization Process of II–VI Compounds*; University of California, Davis: Davis, CA, **1979**.

44. Cline, C. F.Elastic Constants of Hexagonal BeO, ZnS, and CdSe *J. Appl. Phys.* **1967**, 38, 1944[CrossRef], [CAS]

45. Zharnikov, M.; Frey, S.; Heister, K.; Grunze, M.Modification of Alkanethiolate Monolayers by Low Energy Electron Irradiation: Dependence on the Substrate Material and on the Length and Isotopic Composition of the Alkyl Chains *Langmuir* **2000**, 16, 2697– 2705[ACS Full Text ◆], [CAS]

46. Nandwana, V.; Subramani, C.; Yeh, Y.-C.; Yang, B.; Dickert, S.; Barnes, M. D.; Tuominen, M. T.; Rotello, V. M.Direct Patterning of Quantum Dot Nanostructures via Electron Beam Lithography *J. Mater. Chem.* **2011**, 21, 16859[CrossRef], [CAS]

47. Miszta, K.; Greullet, F.; Marras, S.; Prato, M.; Toma, A.; Arciniegas, M.; Manna, L.; Krahne, R.Nanocrystal Film Patterning by Inhibiting Cation Exchange via Electron-Beam or X-ray Lithography *Nano Lett.* **2014**, 14, 2116– 2122[ACS Full Text], [PubMed], [CAS]

DISCLAIMER